Published in final edited form as:
J Mater Chem B Mater Biol Med. 2014 December 14; 2(46): 8116–8122. doi:10.1039/C4TB01487A.

Improved cell infiltration of highly porous nanofibrous scaffolds formed by combined fiber-fiber charge repulsions and ultra-sonication

Sung Isn Jeong[1,#,*], **Nancy A. Burns**[3,*], **Christopher A. Bonino**[3,*,&], **Il Keun Kwon**[4], **Saad A. Khan**[3], and **Eben Alsberg**[1,2,†]

[1]Department of Biomedical Engineering, Case Western Reserve University, Cleveland, Ohio

[2]Department of Orthopaedic Surgery, Case Western Reserve University, Cleveland, Ohio

[3]Department of Chemical & Biomolecular Engineering, North Carolina State University, Raleigh, North Carolina

[4]Department of Maxillofacial Biomedical Engineering, School of Dentistry, Kyung Hee University, Seoul, Republic of Korea

Abstract

A significant problem affecting electrospun nanofibrous tissue scaffolds is poor infiltration of cells into their three-dimensional (3D) structure. Environmental and physical manipulation, however, can enhance cellular infiltration into electrospun scaffolds. In this work, RGD-modified alginate mats with increased thickness and porosity were achieved by pairing high humidity electrospinning with post-processing ultra-sonication. RGD-modified alginate, polyethylene oxide (PEO), and an FDA-approved, nonionic surfactant blends were electrospun in 20 and 50% relative humidity conditions. Mats electrospun in high humidity conditions resulted in significantly increased mat thickness and decreased fiber diameters. The mats' alginate content was then isolated *via* ionic crosslinking and PEO/surfactant extraction. Finally, the alginate-only mat was post-processed by ultra-sonication to further enhance its cross-sectional thickness. Cell morphology, proliferation, and infiltration into the scaffolds were evaluated by seeding fibroblasts onto the alginate mat. Cell spreading, growth and infiltration improved with increased humidity and ultra-sonication. This approach shows great promise for the design of cell-permeable nanofibrous scaffolds for tissue-engineering applications.

1. Introduction

Regenerative medicine has benefited from nanomaterials with tunable biochemical compositions, degradability, mechanical properties and architectures that can serve as scaffolds for transplanted or recruited host cells. These materials may promote cell

[†]To whom correspondence should be addressed; eben.alsberg@case.edu; ph:(216) 368-6425.
[#]current address: Advanced Radiation Technology Institute, Korea Atomic Energy Research Institute, 1266 Sinjeong-dong, Jeongeup-si Jeollabuk-do, 580-185, Republic of Korea
[&]current address: RTI International, Durham, NC, 27709, USA
[*]Co-first authors

behaviors such as adhesion, infiltration, proliferation and/or differentiation as a means to enhance repair or replacement of damaged tissues and organs.[1] Moreover, approaches aimed at mimicking the extracellular matrix (ECM) require a scaffold with a highly porous architecture that also provides structural support for growing tissues. Nanofibrous mats produced by electrospinning are ideal candidates for tissue scaffolds, due to their tunable surface area, high overall porosity (around 80%) and interconnected fibrous structures which resemble the ECM.[2–4] Furthermore, a vast number of biocompatible polymeric materials can be electrospun to support a variety of cell types.[5] Yet, scaffolds fabricated by conventional electrospinning techniques have substantial limitations. Typical subcellular spacing between electrospun fibers can obstruct cell infiltration. Thin mat depths restrict the cell growth structure to a two-dimensional topography.[4–9]

Several strategies have been pursued to address these shortcomings, with mixed results.[10–16] Increasing fiber diameters or combining nano- and micro- scale fibers have resulted in mats with larger pore sizes and thicker dimensions.[4,17] However, these methods produce mats that are less similar in structure to natural ECMs.[18] Other approaches utilize sacrificial particles or microfibers as templates to enhance porosity.[2,17,19–20] These methods have great potential, yet are prone to structural collapse and material loss due to template removal, with only modest thickness enhancements.

The choice of an appropriate electrospinning material is also vital to tissue scaffold performance. Several synthetic polymers (e.g., poly(ε-caprolactone), polylactide and polyglycolide) have been electrospun for tissue engineering applications.[5,21] However, these systems typically require cytotoxic organic solvents and intensive purification steps. Water-soluble biopolymers, such as sodium alginate, are an attractive alternative.[22–24] Sodium alginate is a biodegradable, naturally-derived polysaccharide that has been widely used in drug delivery and tissue engineering applications.[25–26] It can be rendered water insoluble *via* ionic-crosslinking with divalent cations (e.g., Ca^{2+}), therefore eliminating the need for cytotoxic crosslinkers.[27] Non-adhesive to cells in its native form, alginate-based systems can be modified with amino acid sequences containing cell adhesion ligands, such as arginine-glycine-aspartic acid (RGD), to regulate cell adhesion by providing integrin-binding sites.

Native and RGD-modified alginate nanofibers have been obtained by electrospinning with polyethylene oxide (PEO) as a carrier polymer (e.g.,).[9,28] With simple electrospinning modifications and post-electrospinning techniques the desired alginate mat properties can be enhanced for superior cell infiltration without introducing cytotoxicity concerns. For instance, the humidity of the surrounding electrospinning environment can be modulated to increase charge density and fiber-fiber charge repulsions that exist due to the surface charges on the negatively charged alginate to produce self-supported 3D alginate nanofiber mats.[29] Thick, highly porous mats can also be achieved by mechanically separating nanofibers *via* ultra-sonication in aqueous solutions to expand existing pores for increased mat porosity and thickness.[4]

In this paper, we electrospun three-dimensional (3D), highly porous, cell adhesion peptide-modified alginate scaffolds to improve cell adhesion, infiltration and proliferation. The novel approach implemented to fabricate these scaffolds combines the benefits of humidity

enhanced charge repulsion with those of ultra-sonication to increase mat thickness from submicron to millimeter scale while simultaneously improving mat porosity and pore size. The resultant materials maintained this 3D architecture during handling and when submerged in cell media. The impact of increasing mat porosity and thickness was monitored to examine the influence on cell infiltration and proliferation.

2. Materials and Methods

2.1 Materials

Dulbecco's modified Eagle's medium (DMEM), 4′,6-diamidino-2-phenylindole (DAPI), fetal bovine serum (FBS) and antibiotics (penicillin–streptomycin) were purchased from Gibco (Grand Island, NY). Human dermal fibroblasts (HDF) were purchased from ATCC (Manassas, VA). Polyethylene oxide (PEO, 600 kDa, Dow), ethanol, calcium chloride, and Pluronic F127 were purchased from Sigma Aldrich (St. Louis, MO). Protanal LF 20/40 sodium alginate (196 kDa) was generously provided by FMC BioPolymers (Philadelphia, PA) and its molecular weight was reduced to 37 kDa by gamma irradiation (5 Mrad), as previously described.[30] RGD-modified low molecular weight alginate (henceforth called alginate) was synthesized as previously described using the peptide glycine – arginine – glycine – aspartic acid – serine – proline (GRGDSP, Commonwealth Biotechnologies, Richmond, VA).[28]

2.2 Electrospinning

Electrospinning solutions were made by mixing aqueous stock solutions of 4 wt % PEO and 13.5 wt % alginate (37 kDa) with the nonionic surfactant Pluronic F127 for 1 day at 37 °C. The addition of the FDA approved Pluronic F127 at low concentrations minimizes bead defects that are characteristic of electrospun alginate systems without introducing cytotoxicity concerns.[31] The composition of the final electrospinning solution was 10.6/0.8/1.5 wt. % alginate/PEO/Pluronic F127 in water. To electrospin, the blend solution was loaded into a plastic syringe (Henke Sass Wolf, Tuttlingen, Germany) fitted with a blunt-end needle (20G, NanoNC, Inc., Seoul, Korea) and secured to an infusion syringe pump (Model 22, Harvard Apparatus Inc., Holliston, MA). A rotating mandrel (10 cm diameter, 25 cm length; NanoNC, Inc.) covered with aluminum foil was used for collection. The high-voltage power supply (AU 60PO; Matsusada, Inc., Kusatsu, Japan), mandrel, and syringe pump were placed in a plastic glove box to maintain relative environmental humidity at 20 or 50%. Relative humidity (RH) within the chamber was monitored using a Thermo-hygrometer (Fisher, Pittsburgh, PA) and adjusted by flowing dry air either directly into the chamber or into a water-filled flask to decrease or raise the humidity, respectively. Solutions were electrospun for 5 h onto the rotating mandrel at a fixed collection distance (15 cm) and flow rate (0.02 ml min^{-1}) with an applied voltage between 11–13 kV. Circular disks were obtained from the resulting mat samples using a 20 mm diameter punch and air dried overnight before further processing.

2.3 Post Processing

The alginate mats were rendered water insoluble *via* ionic crosslinking with calcium chloride as previously described in the literature.[28,32] Briefly, samples were immersed and

slowly shaken for 10 s in a 100 ml solution of calcium chloride (2 % w/v) dissolved in a water/ethanol mixture (1:5 v/v ratio). Mats were rinsed three times in water to remove any residual chemicals, frozen, and then lyophilized. PEO and Pluronic F127 content was extracted *via* shaking immersed mats in 5 ml water (37 °C) for 5 days to produce alginate-only mats. The ultra-sonicated mats were produced by immersing alginate-only mats in 30 ml deionized water (21 °C) and ultra-sonicating (Branson™ Bransonic Model 2510, 40 KHz, Rochester, NY) for 5 h.

The fiber morphology and cross-sectional analysis of the original alginate/PEO/Pluronic F127, post-extraction alginate-only, and post ultra-sonicated mats were assessed by scanning electron microscopy (SEM; Hitachi S-4500, Tokyo, Japan) at 5 kV. Each sample was prepared by sputter coating with gold (E-1030, Hitachi). Mat cross-sectional thickness (40 times magnification, N=4) and fiber diameters (average of 100 different fibers) were measured using image analysis software (Image-Pro Plus 6.0, Bethesda, MD).

2.5 *In vitro* cell cultures

Primary human dermal fibroblasts (HDFs, American Type Culture Collection, Manassas, VA) were cultured in Dulbecco's modified Eagle medium with 4.5 g/L glucose (DMEM-HG, Hyclone, Logan, UT) supplemented with 10 % fetal bovine serum (FBS, Hyclone) and 1% v/v penicillin/streptomycin (P/S; Hyclone) at 37 °C in a humidified incubator with 5% CO_2, and used for the cell infiltration studies. HDFs (1×10^6 cells/scaffold) suspended in 0.1 ml DMEM containing 10 % FBS were seeded on each alginate scaffold (5×5 mm), and the constructs were then cultured in T-25 flasks with serum containing media for 2 weeks. The culture medium was replaced every 2 days.

To examine the morphology of cells on the scaffolds using SEM, cell-scaffold constructs were fixed using 2.5% glutaraldehyde in ultrapure deionized water (diH2O) at RT for 1 h. After rinsing the samples repeatedly with diH2O, the scaffolds were dehydrated using graded ethanol solutions of 70, 80, 90, and 100% for 30 min at each grading step, lyophilized until dry, sputter coated with gold and imaged by SEM. To investigate cell infiltration, the samples were embedded in freezing medium at −70 °C and cut into 7 μm-thick sections on a cryotome. Sections were stained with hematoxylin and eosin (H&E) and imaged on a Leitz Laborlux S microscope (Leica, Germany) equipped with a digital camera (Coolpix 995, Nikon, Japan). Sections were also stained with 4′,6-diamidino-2-phenylindole (DAPI, Millipore) to visualize nuclei of cells within the constructs. Fluorescence photomicrograph images were acquired using a fluorescence microscope (ECLIPSE TE 300, Nikon, Tokyo, Japan) equipped with a digital camera (Retiga-SRV, Qimaging, Burnaby, BC, Canada).

2.6 Statistics

Data are expressed as mean ± SD. Statistical analysis was carried out with one-way analysis of variance (ANOVA) with Tukey significant difference post hoc test using Graphpad Prism 5.0 software (GraphPad Software, Inc., La Jolla, CA), and a value of $p < 0.05$ was considered statistically significant.

3. Results and discussion

We first examine the morphologies of nanofibrous mats and nanofibers (Figures 1a, b) of low molecular weight, peptide-modified alginate/PEO/surfactant blends electrospun onto a rotating mandrel under two different humidity conditions, low humidity (LH) indicating a RH of 20% and high humidity (HH) indicating a RH of 50%. The humidity conditions were chosen so that uniform fibers could be electrospun and a 3D architecture observed. Electrospinning at humidity conditions lower than 20% results in a flat topology that is typically observed in electrospun mats. On the other hand, higher moisture conditions can cause an accumulation of charge in polyelectrolyte-based polymers, such as alginate, creating fiber-to-fiber repulsions and 3D-mat formation.[29] Raising the RH beyond ~50% results in a slower evaporation rate of an aqueous solvent from an electrospun jet compared to drier conditions, leading to capillary instabilities that manifest as bead defects within the fibers.[29,33] Figures 1a, b reveal that the RH during electrospinning significantly altered the mat thickness and 3D nature. Electrospinning in the LH condition resulted in a consistent, 2D mat coverage around the mandrel with a few areas of thicker 3D growth. In contrast, electrospinning in the HH condition resulted in 3D mat coverage with numerous peaks visible. The cross-sectional thicknesses of the mats were visualized and quantified *via* SEM microscopy (Figures 2a, 2b, and 3a). As expected, the HH mats were significantly thicker (438±68 μm) than the LH mats (18±5 μm). Interestingly, SEM photomicrographs of both LH and HH conditions (Figure 1a and b) showed similar fiber morphology, with uniformly distributed nanofibers and comparable fiber diameters (Figure 3b), which is not consistent with our previous work studying electrospinning of unmodified alginate on a fixed collector plate.[29] These variations are possibly due to differences in experimental setup, such as collection distance or type, or in the peptide modification or purification of the alginate. We have proposed that the 3D fibrous scaffold thickness increase is due to electrospinning high charge density materials where surface charges create repulsion forces between fibers.[34–36] This increased charge density coupled with the “like-charges repulsions between fibers” in alginate cause them to extend off the collector mandrel, thus forming thicker, 3D mats.[29] These thicker mats have reduced fiber density with increased porosity.

An examination of the crosslinking and extraction steps revealed that these steps do not seem to alter fiber morphology, as SEM photomicrographs of samples before (Figures 1a and b) and after (Figures 1c and d) treatment are similar. There was a slight increase in the mat cross-sectional thickness in the alginate-only mats, with LH mats increasing from 18±5 to 29±7 μm and the HH mats increasing from 438±68 to 515±24 μm (Figures 2c, 2d, and 3a). Changes in the fiber diameter were most apparent, with the LH nanofibers decreasing from 229±78 to 128±24 nm and the HH nanofibers decreasing from 177±63 to 122±23 nm (Figure 3b). The statistically-significant decrease in fiber diameters is attributed to the loss of the PEO/Pluronic content during extraction.

The alginate-only mats were subjected to the final processing step of ultra-sonication to increase the porosity and pore size within the scaffold, as well as its overall thickness. Ultra-sonication had little impact on fiber morphology (Figures 1e and f) or diameter (Figure 3b), but drastically decreased the mat’s overall density and doubled the cross-sectional mat thickness (Figures 2e, 2f, and 3a). Specifically, the cross-sectional thickness of the LH mats

increased by more than five times from 29±7 to 150±26 μm, and the thickness of the HH mats more than doubled from 515±24 to 1171±100 μm. The ultra-sonication of the HHs mat created the largest observed pores, on the order of 300 μm, which suggests that combining the ultra-sonication treatment with high humidity electrospinning offers a powerful tool for enhancing porosity. Lee *et al.* reported that thickness increase of electrospun scaffolds after ultra-sonication may be attributed to vibrational energy which allows water to infiltrate into the gaps between the nanofibers and further mechanically agitate them to increase the gaps between the fibers.[4] The increase in mat thickness corresponds to a decrease in mat fiber density and the presence of larger pores, both of which can enable cell migration toward the center of the scaffold.[7,20] It is possible that increased porosity can impact the scaffold's mechanical properties[4]; however we observed no apparent structural collapse or fiber breakage while handling the mats. This lack of noticeable mat damage during handling bodes well for the use of highly porous alginate scaffolds, but mechanical properties need to be examined as part of future work.

Having established that controlled humidity and ultra-sonication can significantly impact mat porosity, density and thickness, the concomitant effect of these mat changes on cell morphology was next investigated. SEM photomicrographs of LH and HH electrospun alginate-only scaffolds with and without ultra-sonication treatments were obtained after culturing cells on them for 2 weeks (Figure 4). LH scaffolds with and without ultra-sonication (Figure 4a and c) exhibited similar cell morphology with many rounded cells visible. Interestingly, the original fiber morphology was not readily apparent on the LH electrospun scaffolds, possibly due to a dense, smooth layer of cells attached to their surfaces. However, individual fiber architecture was apparent when the HH electrospun scaffolds were examined (Figure 4b and d). The difference between the smooth scaffolds observed in the LH conditions versus the fiber-apparent scaffolds in the HH conditions may be attributed to the increased spacing between fibers which increases the volume available for cell migration and proliferation. The increased spacing of fibers in the HH electrospun scaffolds more easily permits visualization of cells that span and interdigitate between the fibers.[37] This interdigitated cell growth was most apparent in the thickest scaffold, HH electrospinning with ultra-sonication treatment, where the cells migrated through the pores, bridged the pore surfaces, appeared more spread and connected fibers in a web like pattern, suggesting that this phenomenon is related to the increased porosity.

High porosity is a desirable attribute for scaffolds as it permits cell infiltration, provides space for cell proliferation and extracellular matrix deposition, and may enhance oxygen and nutrient transport.[18] It was anticipated that the high humidity and ultra-sonication treatments would positively impact cell infiltration as these processes lead to increases in mat thickness and porosity. Cell infiltration into the scaffolds was investigated by examining cross-sectional photomicrographs of DAPI and H&E stained LH and HH electrospun alginate-only scaffolds with and without ultra-sonication treatment. Royal blue dots indicate HDF cell nuclei in DAPI stained scaffolds (Figures 5a–d), and dark purple areas indicate HDFs in H&E stained scaffolds (Figures 5e–h). The LH scaffolds (Figures 5a, c, e and g) displayed cell growth that was predominantly limited to the scaffold surfaces, indicated by the dashed lines. The LH, without ultra-sonication scaffolds appeared to have the least amount cell

growth overall with a majority of cells located on the constructs' surface. Cell growth increased in the LH, ultra-sonicated scaffolds, with areas of high cell concentration visible near the surface and the appearance of cells having started to migrate towards the center of the scaffolds. This behavior indicates that even small changes in mat thickness and porosity *via* the ultra-sonication treatment improved cell infiltration. As the mat thickness and porosity increased further with the HH conditions, so did the amount of visible cells within the center of scaffolds. The HH scaffolds with and without ultra-sonication (Figures 5b, d, f and h) exhibited cells that infiltrated to the center of the constructs, possibly due to fiber-guided cell migration and/or the increased porosity and pore size.[2] To a greater extent than the LH scaffolds, there was a noticeable increase in cell density and penetration depth in the center of the HH scaffolds with ultra-sonication compared to those without. These results indicate that the improved architectural characteristics and mat thickness achieved *via* the combination of HH electrospinning conditions with ultra-sonication treatment enhances the cell infiltration and density into the center of the scaffolds.

4. Conclusions

This study demonstrates that combining high humidity electrospinning with ultra-sonication treatment lead to an increase in surface area through a decrease in fiber diameters while simultaneously decreasing mat density and increasing mat thickness by increasing construct porosity and pore size. These mat transformations enhanced cell infiltration and proliferation, possibly due to increased volume for cells to migrate and grow. Furthermore, the proposed process to create highly porous 3D scaffolds is relatively facile and may be extended to other materials beyond the alginate/polyethylene oxide system presented here, thereby offering a versatile strategy to improve cell infiltration of existing electrospun scaffold systems.

Acknowledgments

The authors gratefully acknowledge funding from the National Institutes of Health (R01AR063194, R21AR061265), the Department of Defense Congressionally Directed Medical Research Programs (OR110196).

References

1. Liu X, Ma PX. Ann Biomed Eng. 2004; 32:477. [PubMed: 15095822]
2. Nam J, Huang Y, Agarwal S, Lannutti J. Tissue Eng. 2007; 13:2249–2257. [PubMed: 17536926]
3. Li WJ, Laurencin CT, Catersin EJ, Tuan RS, Ko FK. J Biomed Mate Res. 2002; 15:613–621.
4. Lee JB, Jeong S, Bae MS, Yang DH, Heo DN, Kim CH, Alsberg E, Kwon K. Tissue Eng. 2011; 17:2695–2702.
5. Goh Y, Shakir I, Hussain R. J Mater Sci. 2013; 48:3027–3054.
6. Eichhorn SJ, Sampson WW. J Roy Soc Interface. 2005; 2:309–318. [PubMed: 16849188]
7. Ranucci CS, Kumar A, Batra SP, Moghe PV. Biomaterials. 2000; 21:783–793. [PubMed: 10721747]
8. Blakeney B, Tambralli A, Anderson J, Andukuri A, Lim D, Dean D, Jun H. Biomaterials. 2011; 32:1583–1590. [PubMed: 21112625]
9. Bhattarai N, Li Z, Edmondson D, Zhang M. Adv Mater. 2006; 18:1463–1467.
10. Zhang H, Jia X, Han F, Zhao J, Zhao Y, Fan Y, Yuan X. Biomaterials. 2013; 34:2202–2212. [PubMed: 23290468]

11. Yang W, Yang F, Wang Y, Both SK, Jansen JA. Acta Biomater. 2013; 9:4505–4512. [PubMed: 23059416]
12. Coburn JM, Gibson M, Monagle S, Patterson Z, Elisseeff H. Proc Natl Acad Sci USA. 2012; 109:10012–10017. [PubMed: 22665791]
13. Ekaputra AK, Prestwich GD, Cool SM, Hutmacher SDW. Biomaterials. 2011; 32:8108–8117. [PubMed: 21807407]
14. Bosworth LA, Alam N, Wong JK, Downes S. J Mater Sci: Mater Med. 2013; 24:1605–1614. [PubMed: 23504088]
15. Cheng Q, Lee BL, Komvopoulos K, Li S. Biomacromoecules. 2013; 14:1349–1360.
16. Cai S, Xu H, Jiang Q, Yang Y. Langmuir. 2013; 29:2311–2318. [PubMed: 23390966]
17. Rnjak-Kovacina J, Weiss AS. Tissue Eng. 2011; 17:365–372.
18. Ma, PX.; Langer, R. Tissue Engineering Methods and Protocols Methods in Molecular Medicine. 1. Morgan, JR.; Yarmush, ML., editors. Vol. 18. Humana Press; New Jersey: 1999. p. 47-56.ch. 4
19. Skotak M, Ragusa J, Gonzalez D, Subramanian A. Biomed Matter. 2011; 6:1–10.
20. Baker BM, Gee AO, Metter RB, Nathan AS, Marklein RA, Burdick JA, Mauck RL. Biomaterials. 2008; 29:2348–2358. [PubMed: 18313138]
21. Pham QP, Sharma U, Mikos AG. Tissue Engineering. 2006; 12:1197–1211. [PubMed: 16771634]
22. Krishnan R, Sundarrajan S, Ramakrishna S. Macromolecular Materials and Engineering. 2013; 298:1034–1058.
23. Lee KY, Jeong L, Kang YO, Lee SJ, Park WH. Adv Drug Delivery Reviews. 2009; 61:1020–1032.
24. Schiffman JD, Schauer CL. Polymer Reviews. 2008; 48:317–352.
25. Goh CH, Heng PWS, Chan LW. Carbohydrate Polymers. 2012; 88:1–12.
26. Sun JC, Tan HP. Materials. 2013; 6:1285–1309.
27. Smidsrod O, Skjakbraek G. Trends in Biotechnology. 1990; 8:71–78. [PubMed: 1366500]
28. Jeong S, Krebs M, Bonino C, Khan S, Alsberg E. Macromolecular Bioscience. 2010; 10:934–943. [PubMed: 20533533]
29. Bonino C, Efimenko K, Jeong S, Krebs M, Alsberg E, Khan S. Small. 2012; 8:1928–1936. [PubMed: 22461238]
30. Alsberg E, Kong H, Hirano Y, Smith M, Alberiruti, Mooney D. J of Dental Research. 2003; 82:903–908.
31. Khattak SF, Bhatia SR, Roberts SC. Tissue Engineering. 2005; 11:974–983. [PubMed: 15998236]
32. Bonino C, Krebs M, Saquing C, Jeong S, Shear K, Alsberg E, Khan S. Carbohydrate Polymers. 2011; 85:111–119.
33. Tripatanasuwan S, Zhong ZX, Reneker DH. Polymer. 2007; 48:5742–5746.
34. Sun B, Long YZ, Yu F, Li MM, Zhang HD, Li WJ, Xu TX. Nanoscale. 2012; 4:2134–2137. [PubMed: 22344309]
35. Lee S, Cho S, Kim M, Jin G, Jeong U, Jang J. Applied Materials and Interfaces. 2014; 6:1082–1091. [PubMed: 24393142]
36. Okuzaki H, Takahashi T, Miyajima N, Suzuki Y, Kuwabara T. Macromolecules. 2006; 39:4276–4278.
37. Min B, Lee G, Kim S, Nam Y, Lee T, Park W. Biomaterials. 2004; 24:1289–1297. [PubMed: 14643603]

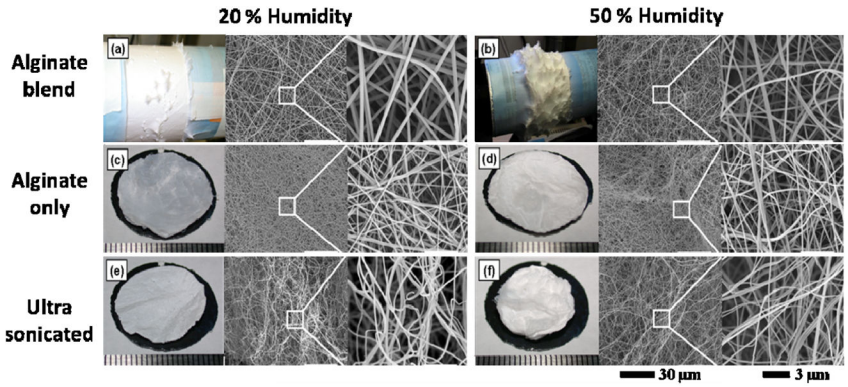

Figure 1.

Photographs and SEM photomicrographs of the top surface of electrospun (a–b) alginate/PEO/Pluronic F127 blended nanofibers, (c–d) alginate only nanofibers following PEO-Pluronic F127 extraction, and (e–f) ultra-sonicated alginate-only nanofibers fabricated at 20% and 50% humidity conditions.

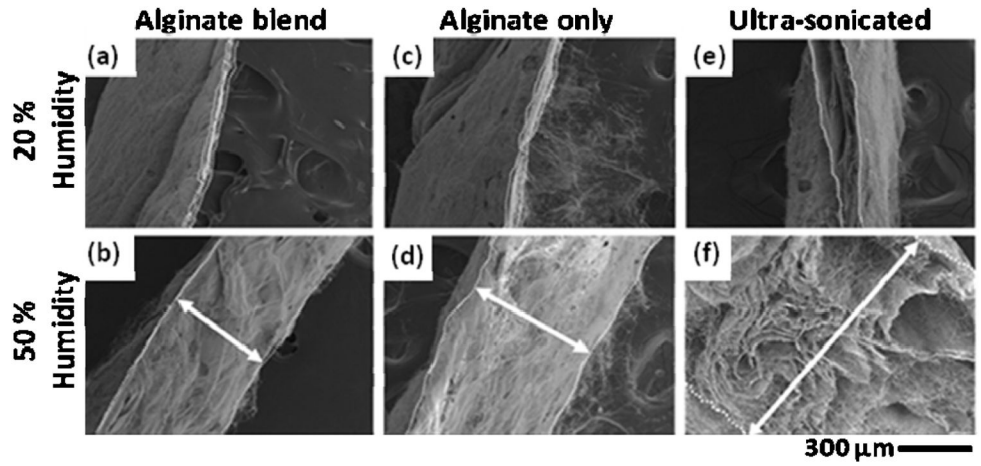

Figure 2.

SEM photomicrographs of cross-sectional sliced mats of (a–b) alginate-PEO-Pluronic F127 blended nanofibers, (c–d) alginate only nanofibers following PEO-Pluronic F127 extraction, and (c, f) ultra-sonicated alginate only nanofibers fabricated at 20% and 50% humidity conditions.

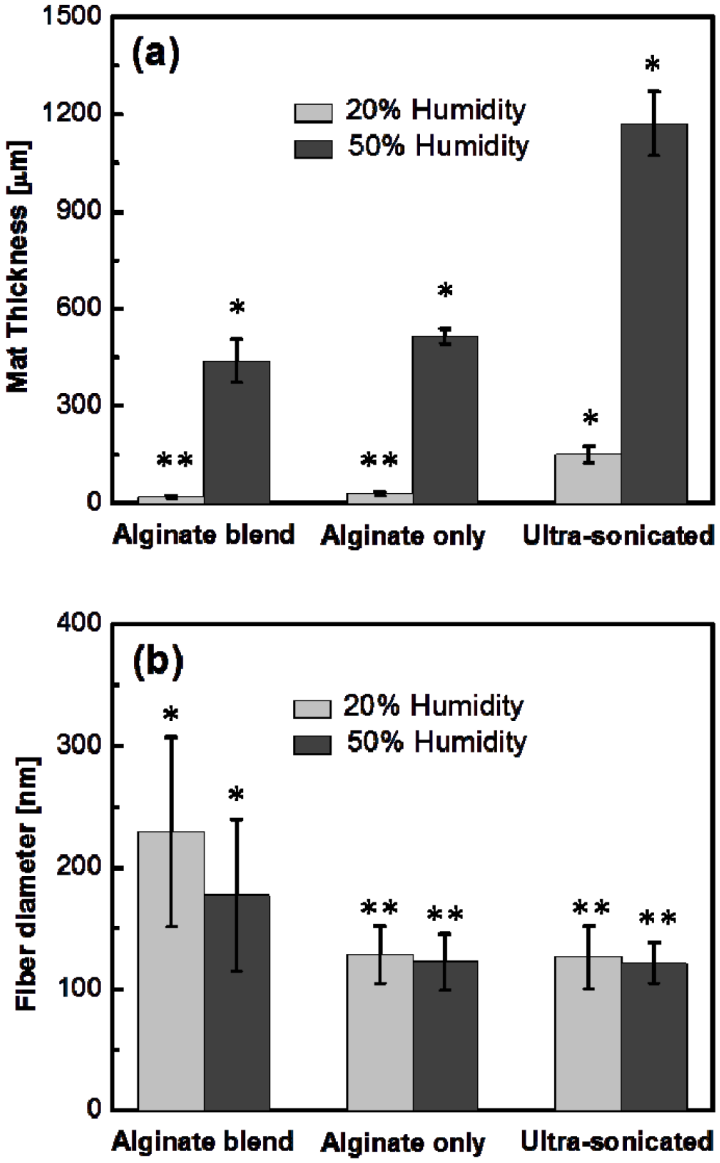

Figure 3.

The average (a) mat thickness and (b) fiber diameter of alginate-PEO-Pluronic F127 blended nanofibers, alginate-only nanofibers following PEO-Pluronic F127 extraction, and ultrasonicated alginate-only nanofibers fabricated at 20% and 50% humidity conditions. * indicates statistically different ($p < 0.05$) from all other conditions. ** indicates statistically different ($p < 0.05$) from all other conditions, except for other **.

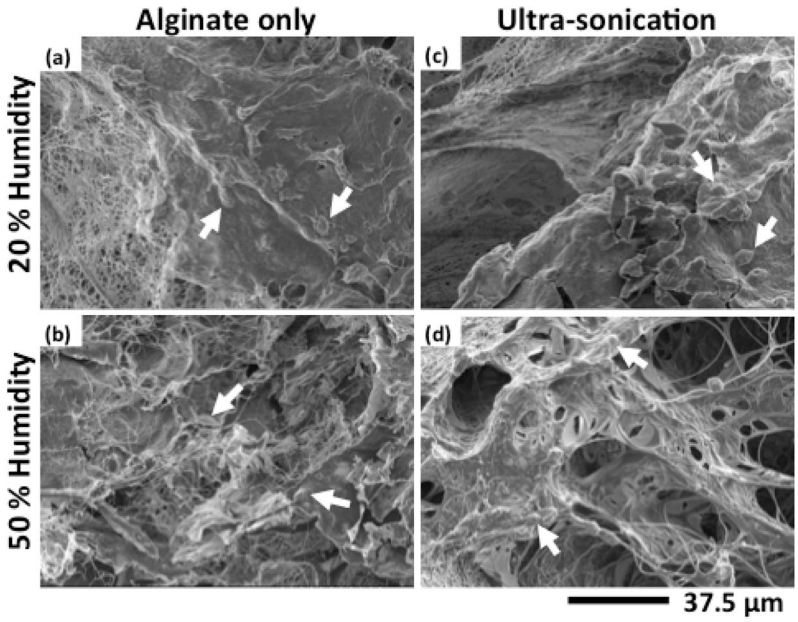

Figure 4.

SEM photomicrographs of HDF seeded (a–b) alginate-only nanofibers following PEO-Pluronic F127 extraction and (c–d) ultra-sonicated alginate-only nanofibers fabricated at 20% and 50% humidity conditions after two weeks of culture. Arrows indicate what are likely some of the cells on these materials.

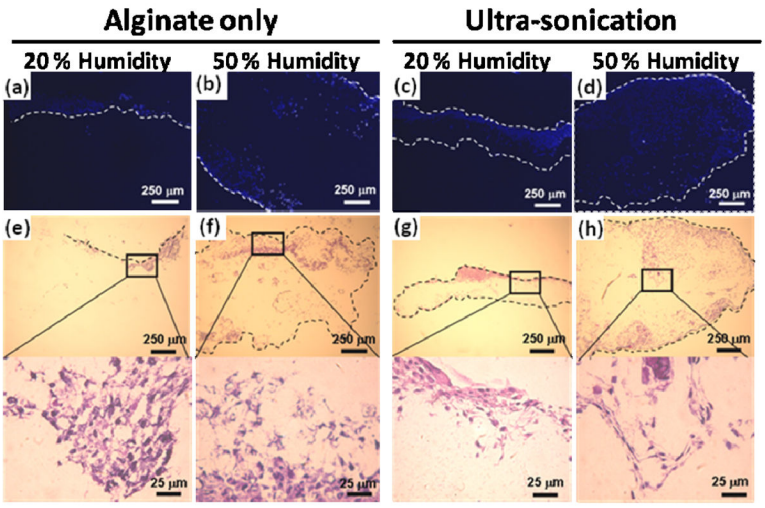

Figure 5.

Fluorescence photomicrographs of DAPI or H&E staining HDF seeded (a–b, e–f) alginate-only nanofibers following PEO-Pluronic F127 extraction and (c–d, g–h) ultra-sonicated alginate-only nanofibers fabricated at 20% and 50% humidity conditions after two weeks of culture.